Excitation and characterization of image potential state electrons on quasi-free-standing graphene

Yi Lin, Yunzhe Li, Jerzy T. Sadowski, Wencan Jin, Jerry I. Dadap, Mark S. Hybertsen, and Richard M. Osgood, Jr.

Phys. Rev. B **97**, 165413 — Published 9 April 2018

DOI: 10.1103/PhysRevB.97.165413

Excitation and Characterization of Image Potential State Electrons on Quasi-Free-Standing Graphene

Yi Lin,[1] Yunzhe Li,[1,*] Jerzy T. Sadowski,[2] Wencan Jin,[1,†] Jerry I. Dadap,[1] Mark S. Hybertsen,[2] and Richard M. Osgood, Jr[1]

[1] *Columbia University, New York, New York 10027, USA*
[2] *Brookhaven National Laboratory, Upton, New York 11973, USA*

(Dated: March 13, 2018)

We investigate the band structure of image potential states in quasi-free-standing graphene (QFG) monolayer islands using angle-resolved two-photon-photoemission spectroscopy (AR-2PPE). Direct probing by low-energy electron diffraction (LEED) shows that QFG is formed following oxygen intercalation into the graphene-Ir(111) interface. Despite the apparent decoupling of the monolayer graphene from the Ir substrate, we find that the binding energy of the n=1 image potential state on these QFG islands increases by 0.17 eV, as compared to the original Gr/Ir(111) interface. We use calculations based on density functional theory to construct an empirical, one-dimensional potential that quantitatively reproduces the image potential state binding energy and links the changes in the interface structure to the shift in energy. Specifically, two factors, arising from the presence of intercalated oxygen adatoms, contribute comparably to this energy shift: a deeper potential well and the increase in the graphene-Ir distance associated with a wider potential well. While image potential states have not been observed previously on QFG by photoemission, our work now demonstrates that they may be strongly excited in a well-defined QFG system produced by oxygen intercalation. This opens an opportunity for studying the surface electron dynamics in QFG systems, beyond those found in typical non-intercalated graphene-on-substrate systems.

I. INTRODUCTION

Because of its importance for understanding interfacial physics, there has recently been a growing interest in intercalated graphene systems, including studies of the occupied states using a plethora of probes. These studies have shown an interesting series of subtle and unexpected surface phenomena in the intercalated graphene substrate system, including the decoupling of the graphene-substrate interaction and modulation of the graphene electronic structure near the Dirac cone[1–3], the loss of the interfacial moiré pattern and surface corrugation in the presence of intercalation[4–7], and the effects of graphene in protecting the vulnerable surface states on a metal substrate[8–10], even in the presence of intercalated adatoms[11].

The response of the empty states in the intercalated graphene has been, in general, much less studied. A particularly fruitful approach has been based on processes in which electrons transiently occupy image potential states (IPS). The IPS broadly occur at dielectric and metal surfaces, and various measurement techniques yield well-defined photoemission spectral features[12–22]. Of course, these studies have been used to characterize IPS themselves at graphene/metal interfaces[23–26] and more recently intercalated graphene systems. For example, angle-resolved-two-photon-photoemission (AR-2PPE) measurements of the IPS on the graphene on Ir(111) system (Gr/Ir), revealed the evolution of the binding energy with the coverage of graphene[23]. In addition, the change in work function could be measured and the characteristics of the initial, Ir-surface-derived states were inferred. These properties of the IPS can be understood from an effective 1D model potential that captures both the image potential outside the surface and its extension into the physical material surface[26–28]. However, a recent study of IPS on the Gr/SiC interface illustrates the challenges that may be encountered in the presence of intercalated atoms[26,29]. In this case, upon hydrogen intercalation at the interface, the previously strong IPS photoemission signal disappeared, likely as a result of the pumping process being rendered ineffective[24,30,31]. It is thus of pressing interest to use the insights from AR-2PPE measurements to investigate fully the response of the normally unoccupied states to intercalation of the graphene/metal interface with atoms as well as its corresponding deintercalation. In particular we make use of chalcogen atoms as the intercalants for this interfacial system.

In this paper, we report on the direct band-structure mapping of IPS in oxygen-intercalated and deintercalated graphene on an Ir(111) single-crystal substrate. Our AR-2PPE measurements and supporting theoretical calculations probe the changes in the characteristics of IPS upon oxygen intercalation. We find that the IPS are bound more strongly to graphene islands or graphene regions on the substrate as a result of intercalation. Our experiments measure the evolution of the band structure, including binding energy shifts in the n=1 IPS and the effective mass of this same state as a result of oxygen intercalation and deintercalation. Finally, using input from density functional theory calculations, we expand on a recently proposed one-dimensional model for IPS to explain the observed changes in IPS binding energy upon oxygen intercalation.

II. METHODS

A. Experimental

The samples for our experiments were prepared in situ both at Columbia University and at Brookhaven National Laboratory (BNL). Initially, the bare Ir(111) surface was prepared via several cycles of Ar-sputtering and annealing in vacuum and in the presence of oxygen, and then examined using low-energy electron diffraction (LEED). Subsequently a sub-monolayer of graphene, which consists of graphene islands or patches, was grown on this surface and monitored by LEED using multiple cycles of temperature-programmed growth (TPG). This multi-domain approach was used since small islands increase the efficiency of oxygen intercalation by providing more surface boundaries[32,33]. For each TPG cycle, the Ir crystal was first exposed to ethylene under a partial pressure of 5×10^{-6} Torr for 30 s at room temperature and then flash heated to 1250 K for 30 s. The oxygen intercalation and deintercalation were accomplished by heating the Gr/Ir sample to 550 K in 2×10^{-6} Torr oxygen for 3 min, and then heating this Gr/O/Ir sample to 680 K under ultrahigh vacuum (UHV) for 5 min, respectively. The reproducibility and robustness of the above procedure were confirmed via μ-LEED (with 2μm selected-area aperture) and low-energy electron microscope measurements in the aberration-corrected LEEM (AC-LEEM) at the Center for Functional Nanomaterials at BNL. The LEEM measurements were particularly useful for monitoring the overall surface quality. This same procedure was then applied in our 2PPE photoemission chamber with a standard LEED system at Columbia University. Under the same growth conditions, identical results were obtained with the BNL and Columbia preparation chambers. The 2PPE experiments were carried out immediately following sample preparation at room-temperature sample.

Our photoemission laser system made use of an ultrafast Ti:Sapphire oscillator whose pulses were amplified in a regenerative amplifier and then used to drive an optical parametric amplifier to provide a tunable source of visible light. The visible output pulses were first frequency-doubled in a β-BaB_2O_4 nonlinear crystal, which produced a train of tunable UV, sub-100 fs pulses, with photon energies in the 3.6-5.1 eV range at a 250 kHz repetition rate and a pulse energy of 10 nJ in an estimated spot size of 200 μm. Prior to entrance of the UV pulses into the UHV chamber, the temporal profile of the UV pulse was optimized using a prism pair to maximize the 2PPE electron counts. The photoemitted electrons were collected using a 160° spherical-sector energy analyzer having a $k_{||}$ momentum resolution of 0.03 $Å^{-1}$ and an energy resolution set to 50 meV. The incidence angle of the laser beam was fixed at 70° and the detector was rotated about the fixed sample. Our sample was biased at -0.5 V to reduce the effects of stray electric fields in the vicinity of the sample.

B. Theoretical

In order to clarify the origin of the increase in binding energy of IPS due to oxygen intercalation, we theoretically explored the impact of interfacial region structure on an effective one-dimensional (1D) potential model describing the IPS. This model advances on that proposed by the Höfer group[28]. They only consider the non-intercalated case and combine an analytical 1D-potential model for the metal surface[27] with a fitted model potential representing LDA plus image potential effects for graphene[34]. Two of the parameters describing the metal surface are fitted to optimize the lowest IPS energy. Then, with this model, they were able to describe the evolution of the IPS and interface states at the metal/graphene interface and to demonstrate quantitative agreement with many experimental observations[28,35]. An alternative approach to compute an effective 1D-potential for graphene, based on the dielectric response, has been explored[36], but not yet applied to the more complex metal-graphene systems.

Here, we build on the approach by the Höfer group[28] in a way that allows us to include the impact of intercalation of oxygen atoms at the Gr/Ir(111) interface. First, the interface structure and work function are determined for each surface and interface under study using density functional theory based calculations. Specifically, the Ir(111) surface is modeled using a 2×2 surface unit supercell and a periodically repeated slab model consisting of 6 monolayers of Ir atoms and a vacuum layer of 30 Å thickness. The coverage of O adatoms is set to 25% for the O/Ir(111) calculation. The calculations were carried out with CASTEP[37] using the local density approximation (LDA) and ultrasoft pseudopotentials contained in version 7.2.1[38]. A plane-wave basis set, truncated with a 600 eV energy cutoff, is used. A periodic dipole correction is applied in a self-consistent manner. The local geometry is optimized for the uppermost Ir layer and the oxygen adatoms.

For calibration, we compare our calculated bulk Ir and relaxed Ir(111) and O/Ir(111) surface structures to previous DFT-based results from the literature[39,40]. With LDA, we find $a_0 = 3.83$ Å, compared to 3.86 Å (Perdew-Wang-91, PW91)[39], 3.85 Å (Perdew-Burke-Ernzerhof, PBE)[40], and 3.84 Å (experiment quoted in[40]). The specific form of gradient corrected exchange-correlation functional used is noted. The deviations from experiment are quite small in all cases and fall well within expected bounds. Our computed spacing between the surface and subsurface layer of Ir(111) is 2.17 Å with the bulk layer spacing being 2.21 Å as compared to previous PBE results of 2.19 Å for the surface layer and 2.22 Å for the bulk[40].

Using the calculated Fermi energy and the potential averaged parallel to the slab, we calculate the work func-

tion for Ir and 25% O/Ir and find them to be 5.79 eV and 6.08 eV, respectively. These results agree with the experimental Ir work function at 5.79 eV[41] and the calculated 25% O/Ir work function at 6.04 eV[39].

We also consider model structures for Gr/Ir and Gr/O/Ir, in which the graphene is stretched to match the Ir(111) surface-lattice parameter. We probed the position of the model graphene layer at the Ir and O/Ir interfaces, finding 3.48 Å and 3.80 Å separation from the top-most Ir layer (average) vertical position, respectively. In this case, the LDA is augmented by the OBS correction[42] to approximate van der Waals interactions. Our calculated average vertical distances are in reasonable agreement with results from the literature. X-ray standing wave measurements gave 3.38±0.04 Å for Gr/Ir(111)[43]. DFT-based computations with a 9×9 Ir supercell matched to 10×10 graphene resulted in an average height of 3.41 Å[43]. Another calculation based on an 8×8 Ir supercell matched to 9×9 graphene gave 3.53 Å for Gr/Ir and 4.02 Å for Gr/O/Ir[44]. Finally, results for a much smaller supercell $\sqrt{3}\times\sqrt{3}$ rotated 30 degrees matched to 2×2 graphene gave 3.48 Å and 3.81 Å for Gr/Ir and Gr/O/Ir, respectively[45]. All of these DFT results also included consideration of van der Waals interactions, the detail of which can be found in the original references.

To obtain a complete 1D potential for the system with graphene that best represents the Gr/Ir and Gr/O/Ir interfaces and the image potential characteristics, we start from self-consistent DFT results for Ir(111) and O/Ir(111) respectively, averaging parallel to the surface. We fit these results to the analytical model of Chulkov and coworkers[27] which includes an image potential tail. In previous work, the Höfer group fit four parameters in that model empirically, in part, to reproduce the experimental IPS binding energies[28]. Instead, we use the DFT results to establish the model, with no free parameters as such. Further, this allows us to systematically include the role of oxygen in the same procedure. Then we join the Ir(111) and O/Ir(111) potentials with the graphene potential of Silkin and coworkers[34], following the procedure of the Höfer group. The final potential includes their higher-order image charge correction and work function correction[28]. This approach then yields a 1D model potential for Gr/Ir and Gr/O/Ir. Solution of the Schrödinger equation in 1D with this potential gives the binding energy and surface-normal electron density distribution for the IPSs. Further details of our potential construction are illustrated in the Section B of the Supplementary Material.

III. RESULTS

A. LEED Characterization of Surface Crystallinity

Our LEED measurements provided critical information on the crystallinity of our samples at key stages of their preparation: (a) clean Ir(111), (b) preintercalated Gr/Ir, (c) oxygen-intercalated Gr/O/Ir and (d) oxygen-deintercalated Gr/Ir. For example, as shown in Fig. 1(a), the hexagonal LEED pattern reflects the excellent crystallinity of clean Ir(111) surface. As shown in the μ-LEED pattern Fig. 1(b), obtained after 8 TPG cycles, a moiré pattern is observed in reciprocal space for the graphene-Ir interface. Based on the distribution of the diffraction spots from graphene and Ir, and the known lattice constant of Ir(111) given by 2.73 Å[46], the lattice constant for the grown graphene is found to be 2.45 Å. After oxygen intercalation, the moiré diffraction spots, shown in Fig. 1(c), weaken in intensity and two aligned hexagonal LEED patterns begin to emerge[47], with inner and outer patterns corresponding to the Ir(111) surface and the graphene layer, respectively. The observed disappearance of the moiré pattern in the presence of oxygen is consistent with the current understanding of the effect of intercalated oxygen on the Gr/Ir interface. In particular, it has been found in prior work that oxygen intercalation releases and lifts up the graphene layer from the substrate and thus decouples the electronic interaction between the graphene and Ir[4–7]; this decoupling leads to the weakening (but not eliminating[44]) of the surface moiré pattern (or periodic corrugation pattern) that arises from the weak interaction between the graphene layer and the Ir(111) surface[8–10]. Our measurements further show that the crystalline lattices of the graphene and the Ir(111) surface are aligned after growth as shown by the two sets of sharp and fully aligned hexagonal LEED patterns in Fig. 1(c). Figure 1(d) shows the effects of oxygen deintercalation on the LEED pattern. In this case, during deintercalation, the moiré pattern reappears, indicating the restoration of the corrugation. Although not shown in our paper, we have observed a 2×2 LEED pattern on oxygen-dosed Ir(111), following the same oxygen treatment that we state in the Methods Section.

Finally note that the appearance, disappearance, and reappearance of the Gr/Ir moiré LEED pattern at the same electron energy (60 eV) provide very reliable and reproducible indicators for monitoring the sample growth, as well as oxygen intercalation and deintercalation. Further details of the evolution of the intercalation and deintercalation processes are provided in Section A of the Supplementary Materials, which includes real-time LEED videos. Also note that similar results were obtained in the two vacuum chambers used in our experiments.

B. AR-2PPE Mapping of IPSs Electronic Structure in Gr/Ir(111) and Gr/O/Ir(111)

In this section, we describe AR-2PPE measurements of the image states for each of our three interfacial systems: preintercalated Gr/Ir, intercalated Gr/O/Ir and deintercalated Gr/Ir. Note that because the pure Ir and O/Ir surfaces have relatively high work functions of 5.79±0.1

eV[25,48] and 6.35±0.04 eV[48], respectively, their image states are not excited using our photon energy of 4.64 eV. In fact, the observed image states are formed only on the graphene-covered surface regions; a discussion of this point is presented in a previous paper[23].

1. *Energy Features*

Figure 2 presents our experimental AR-2PPE mapping of the n=1 and n=2 image potential states centered about $k_{||}$ =0 for the Γ point using an incident photon energy of $\hbar\omega$=4.64 eV. The photoemission spectra in the figure show two important features. First, the energy of the n=1 IPS shifts from 3.86 eV to 4.16 eV above Fermi level following oxygen intercalation. Second, while the energy of the n=2 IPS is 4.46 eV in Gr/Ir and is observed, this image state is not observed on Gr/O/Ir samples for the photon energy used. Measured relative to the vacuum level, these energies indicate the binding energies of the IPS and will be examined more carefully in the Discussion section below.

2. *Spectral Intensity Features*

In the presence of intercalated oxygen, an additional spectral structure is readily observed by examining the variation of the normalized intensity profile

Intercalated oxygen alters key spectral features that can be deduced by examining the normalized intensity profile of the n=1 IPS energy distribution curve (EDC) as a function of $k_{||}$. These are shown for the three different interfaces (see bottom panels of Fig. 2). Specifically, for this image state, a resonance-like feature is observed in the vicinity of $k_{||}$ = 0.14 Å^{-1}. The photoemission intensity increases sharply by a factor of 2 as $k_{||}$ varied from 0 to 0.14 Å^{-1} for the Gr/Ir systems in Fig. 2(a) and (c); in contrast, this behavior is not observed in the case of the intercalated Gr/O/Ir system in Fig. 2(b). Note that for each figure, the data is normalized relative to their values at $k_{||}$ =0.

This behavior can be attributed to changes in the Ir(111) Rashba-split surface states. These states have been investigated extensively for the clean Ir and Gr/Ir surfaces[10]. Earlier studies have conclusively demonstrated the spectral peak structure as arising from a resonant optical transition from the pair of Rashba-split surface states of the iridium substrate to the n=1 IPS of graphene[23,49]. However, the surface states may be strongly perturbed or eradicated by the mere presence of a trace amount of stray surface oxygen adsorbates[50]. Consequently, the resonant excitation channel via the Rashba surface states is extinguished thereby quenching the resonance feature, as shown in Fig. 2(b). Our observation of the extermination and restoration of the resonant peaks due to the absence or presence of the surface states indicates the efficiency of our in situ oxygen inter-

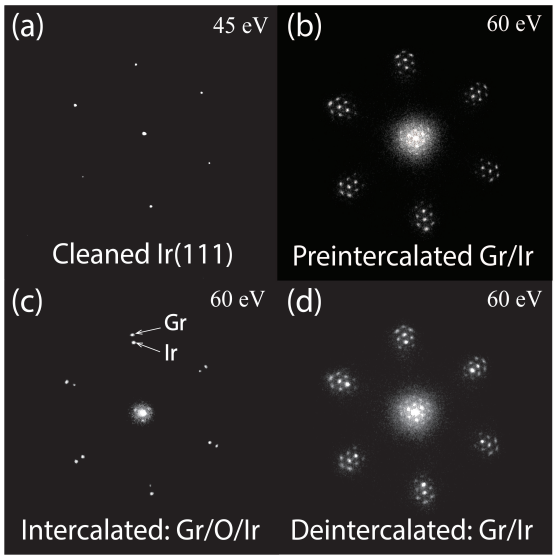

FIG. 1. μ-LEED patterns of (a) cleaned Ir(111), (b) preintercalated Gr/Ir, (c) oxygen-intercalated Gr/O/Ir and (d) oxygen-deintercalated Gr/Ir. The energy label on the top right corner of each subfigure denotes the incident electron kinetic energy. The arrows in (c) indicate the hexagonal diffraction patterns associated with graphene and iridium surfaces.

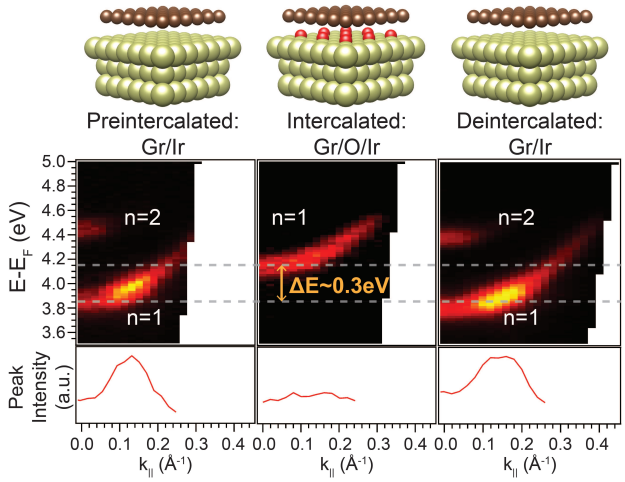

FIG. 2. Image potential state band structure (middle panel) and normalized EDC peak intensity profile (bottom panel) versus parallel momentum for (a) preintercalated Gr/Ir, (b) intercalated Gr/O/Ir and (c) deintercalated Gr/Ir, schematically presented in the top panel. The grey dashed line denotes the energy of n=1 IPS for preintercalated and intercalated systems. The shift in the binding energy of the n=1 IPS, between Gr/Ir and Gr/O/Ir, is ΔE=0.3 eV. Note that in this figure the symmetry point for $k_{||}$ =0 corresponds to the Γ point. The photon energy is $\hbar\omega$=4.64 eV.

calation and deintercalation processes; this same effectiveness is demonstrated in the loss of the moiré pattern, observed in the LEED measurement during intercalation.

3. *Effective Mass Features*

The AR-2PPE data measured above also allows us to determine the effective mass of the measured n=1 IPSs shown in Fig. 2. Using simple parabolic fit to the dispersion[51], we obtain the effective mass for preintercalated Gr/Ir as $m = 0.84\pm0.05\ m_0$, where m_0 denotes the free electron mass. This value is in close agreement with the experimental results obtained in our previous study[23]. In addition, the effective masses for the intercalated Gr/O/Ir and de-intercalated Gr/Ir phases are measured to be $0.86\pm0.05\ m_0$ and $0.84\pm0.05\ m_0$, respectively. These values are close to the values on the pristine surface, which indicates that the IPS states in Gr/Ir interface are sufficiently separated from the surface such that the in-plane surface potential variation due to oxygen intercalation and deintercalation weakly scatters the IPS electrons parallel to the plane of the surface. However, our theoretical model will show that the behavior of the IPS state electrons is heavily influenced by the out-of-plane surface potential variation due to oxygen intercalation; see the Discussion section below.

C. Work Function Measurement for Gr/O/Ir

In this section, we use our experimentally determined work function values to obtain the work function of Gr/O/Ir. Since the oxygen intercalation typically uses partial graphene coverage[50], the measured work function using 2PPE is an average over multiple surface domains, i.e., monolayer (ML) graphene patches. Thus in order to estimate the work function $\Phi_{\mathrm{Gr/O/Ir}}$ of an isolated Gr/O/Ir single domain, i.e., its local work function, we need to disentangle the multi-domain effects using prior experimental results. In particular, the work function of the Gr/Ir domains and of bare Ir were reported as $\Phi_{\mathrm{Gr/Ir}} = 4.65\pm0.10$ eV[23] and $\Phi_{\mathrm{Ir}} = 5.79\pm0.10$ eV[25], respectively, and correspondingly denoted by blue circles and blue squares in Fig. 3. For samples containing monolayer patches of graphene on Ir, the work function measured by 2PPE on a multi-domain sample is a linear combination of the work function of each single domain weighted by the fractional size of each domain[23]. Specifically, the work function for the graphene-Ir system is given by $\Phi = (1-\theta)\Phi_{\mathrm{Ir}}+\theta\Phi_{\mathrm{Gr/Ir}}$, which is denoted by the blue line connecting the blue circle and the blue square in Fig. 3. For an oxygen-saturated Ir domain, its work function is known as $\Phi_{\mathrm{O/Ir}} = 6.35\pm0.04$ eV[48]. As in the case for our oxygen-intercalated system, the work function for an arbitrary coverage of monolayer graphene patches may similarly be written as $\Phi_{\mathrm{interc}} = (1-\theta)\Phi_{\mathrm{O/Ir}}+\theta\Phi_{\mathrm{Gr/O/Ir}}$.

To determine the value of $\Phi_{\mathrm{Gr/O/Ir}}$, our experiments are carried out in three stages indicated by ①, ②, and ③ symbols in Fig. 3, corresponding to the following steps: (1) A preintercalated graphene-Ir system is prepared such that its measured work function is $\Phi = 5.03\pm0.02$ eV, corresponding to a graphene coverage $\theta = 0.67$ ML (upward blue triangle in Fig. 3); (2) oxygen is intercalated and the work function is measured to be $\Phi_{\mathrm{interc}} = 5.54\pm0.02$ eV (clear orange triangles in Fig. 3); and (3) oxygen is deintercalated and the work function is remeasured to be $\Phi = 5.15\pm0.02$ eV, which corresponds to a graphene coverage $\theta = 0.56$ ML (downward blue triangle in Fig. 3).

In Fig. 3, we find that for the pre- and de-intercalated Gr/Ir, the work function increases from 5.03 to 5.15 eV, which corresponds to a loss of graphene coverage of 0.11 ML from 0.67 ML to 0.56 ML. From this information alone, we cannot determine how much of this loss can be identified with a specific step of the intercalation-deintercalation cycle. As a result, there is an uncertainty in the determination of the graphene coverage for the Gr/O/Ir system. We can see from Fig. 3, however, that the exact graphene coverage lies between 0.56 and 0.67 ML. Using the coverage-dependent expression for Φ_{interc} above, we obtain the lower and upper limits for $\Phi_{\mathrm{Gr/O/Ir}}$ to be 4.90 and 5.14 eV, respectively (corresponding to downward- and upward-pointing solid red triangles). Therefore, we find that the intercalation of oxygen in a graphene/Ir system increases its work function, $\Phi_{\mathrm{Gr/Ir}} = 4.65$ eV, by an amount that ranges between 0.25 eV and 0.49 eV. This range is in agreement with the range of the measured work function increase of 0.4±0.1 eV as measured by scanning tunneling spec-

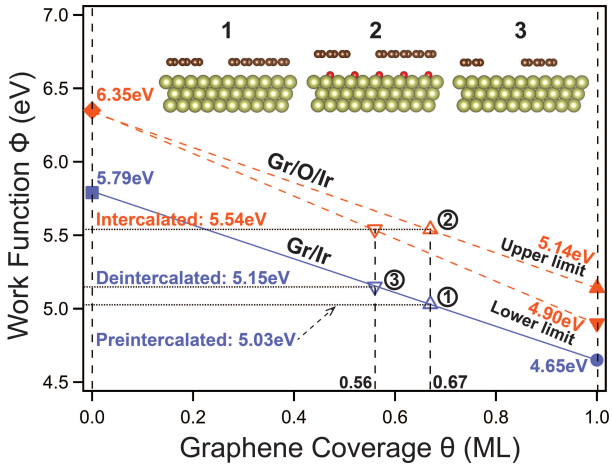

FIG. 3. Schematic showing our calculations to estimate work function of the Gr/O/Ir domains. Work functions were measured at preintercalated, intercalated, and deintercalated stages under submonolayer graphene conditions denoted by ①, ②, ③, respectively. Two measured graphene coverage in the nonintercalated stages determine the upper and lower limit of $\Phi_{\mathrm{Gr/O/Ir}}$ thus yielding 4.90 eV$\leqslant\Phi_{\mathrm{Gr/O/Ir}}\leqslant$5.14 eV. See details in text.

troscopy (STS)[52]. However, to estimate the work function $\Phi_{Gr/O/Ir}$ more accurately, we need to understand the loss of graphene due to its reaction with oxygen during intercalation and deintercalation. Loss of graphene during both processes have been observed, showing that as much as 20% of the graphene may be lost during deintercalation but only 1-2% during intercalation[1,53,54]. Hence, for the rest of our discussion we may assume a $\approx$ 1% graphene loss during oxygen intercalation, from which we estimate that $\Phi_{Gr/O/Ir} \approx 5.12$ eV; this value will be used to derive the binding energies of the IPS below.

IV. DISCUSSION

In this section, we begin by calculating the experimental binding energies of IPS in Gr/Ir and Gr/O/Ir based on the energy and work function measurements presented in the Results section. We then develop an effective potential model that allows us to understand the variation of the IPS binding energy due to oxygen intercalation in the Gr/Ir interface.

The measured IPS energy level with respect to sample Fermi energy ($E - E_f$) and the local work function (Φ) determine the binding energy of the IPS with respect to the vacuum level. For the Gr/Ir region, the local work function is 4.65 eV and the measured energies for n=1 and n=2 IPS are 3.86 eV and 4.46 eV, respectively. Thus, the experimental binding energies of n=1 and n=2 IPS are 0.79 eV and 0.19 eV, with respect to E_v. These values reproduce well the corresponding values of the same states measured in Gr/Ir[23]. The work function of the Gr/O/Ir region is $\approx$ 5.12 eV and our measured energy for the n=1 IPS is 4.16 eV. Therefore, the experimental binding energy of the n=1 IPS in our measurements is estimated to be $\approx$ 0.96 eV. As mentioned in the introduction, it has been widely reported that oxygen intercalation can decouple the graphene from the metal substrate and give rise to quasi-free-standing graphene with a graphene-like Dirac cone band structure. In contrast, the IPS state in the quasi-free-standing system is actually more strongly bound; specifically, the binding energy of the n=1 IPS at 0.79 eV in Gr/Ir increases to 0.96 eV in Gr/O/Ir.

Method	Distance(Å)	Gr/Ir (eV)		Gr/O/Ir (eV)	
		n=1	n=2	n=1	n=2
Theory	3.48	***0.77***	***0.21***	0.87	0.22
	3.80	0.86	0.22	***0.97***	***0.24***
Experiment		***0.79***	***0.19***	***0.96***	
Ref. Th.[a]	3.4	0.88	0.23		
Ref. Exp.[b]		0.83	0.19		

a 28

b 23

TABLE I. Calculated binding energies for the IPS (n=1, 2) in Gr/Ir and Gr/O/Ir interfaces. The results of our 1D potential are compared with the experimental values reported using 2PPE[23] and theoretical values calculated using an analytical 1D potential model[28]. The distance denotes the separation between graphene and Ir surface. Two distance values are specified as a result of DFT-calculated interlayer distances in Gr/Ir (3.48 Å) and Gr/O/Ir (3.80 Å). The theoretical energy values in bold italic font correspond to the IPS probability densities presented in Fig. 4(a) for Gr/Ir and Gr/O/Ir.

Prior experiments have in fact examined the specific details of the intercalation process for oxygen at graphene/Ir interfaces. Prior works have generally concluded that molecular oxygen is first thermally dissociated on Ir sites in order to form chemisorbed O-Ir bonds and these bonds found in intercalation are known to behave chemically in a similar fashion as chemisorbed oxygen on bare Ir[55–59]. These Ir-chemisorbed oxygen atoms then diffuse underneath the graphene islands from their edges until a saturated concentration is reached beneath the islands[32]. As a result of this process, an oxygen-intercalated layer forms and then "lifts" the graphene from the Ir surface, i.e., the graphene-Ir distance increases. Electron transfer from the metal to the chemisorbed oxygen layer fills the oxygen valence states, leaving a residual, van der Waals interaction with the graphene layer above. The displaced or released graphene then forms a quasi-free-standing graphene layer.

In order to clarify the origin of the increase in binding energy of IPS due to oxygen intercalation, we use the one-dimensional potential model to describe the induced changes in the interfacial region, the corresponding modulation of the surface-normal potential, and finally, the evolution of the IPS binding energies and electron probability-density distributions. Figure 4(a) shows the 1D potential that we deduce in each case, along with the IPS electron probability-density distributions. Calculated IPS binding energies are reported in Table I. Our results for Gr/Ir agree quite well with the measured values of binding energy. In our calculation, we do not see even and odd IPS; we attribute this phenomena to the fact the 1D potential is no longer truly symmetric as is the case for free-standing graphene due to the proximity of the substrate and intercalant. The IPS evolution from the even-and-odd manner in freestanding graphene to the manner resembling the one on the semi-infinite surface in Gr/substrate has been discussed in the reference[28].

As a consequence of the oxygen intercalation, intercalated oxygen adatoms form chemical bonds with the Ir surface and the distance between the Ir surface layer and the Gr layer is increased. Our calculations show that these two structural changes result in modifications to the potential profile within the interface. A comparison of this Gr/O/Ir (red) 1D potential with that of the Gr/Ir (blue) potential shows that with oxygen intercalation, two predominant effects arise: a deeper and wider potential well. The former effect is specifically in the vicinity of the O adatoms (see the potential difference around z = 1-2 Å). The latter effect is directly associated with the increased graphene-Ir distance (i.e., see the potential dif-

ference around z = 4-6 Å). As a natural consequence of such a deeper and wider potential well, stronger binding of IPS is seen since the electron probability-densities are closer to the graphene surface as shown in Fig. 4(a), as well as the larger binding energies seen in Table 1. The increase in binding energy of the n=1 IPS upon oxygen intercalation is more pronounced compared to that of the n=2 state because of two factors: the closer proximity of the n=1 image state to the graphene layer as well as its stronger localization. In particular, the change in the binding energies for the n=1 and n=2 IPS are 0.2 eV and 0.03 eV, respectively, after oxygen intercalation, as calculated in our model.

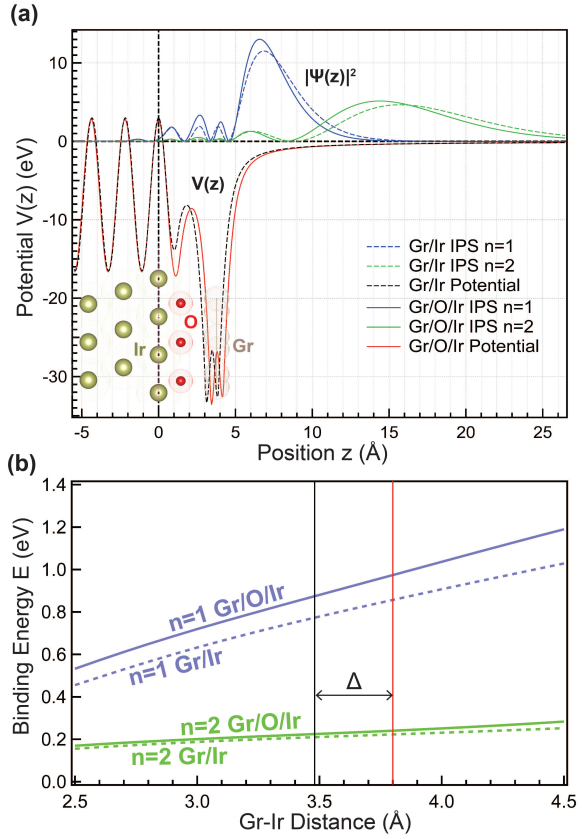

FIG. 4. Panel (a) shows 1D potential model for Gr/Ir and Gr/O/Ir and the corresponding probability densities $|\Psi(z)|^2$ for the IPS. The potentials and states for Gr/Ir and Gr/O/Ir are plotted using dashed line and solid line, respectively. The yellow, red, and brown balls and shades indicate the ideal position of the Ir surface, the intercalated oxygen adatoms, and the graphene layer at the Gr/O/Ir interface, respectively. The horizontal axis denotes the position z along the direction perpendicular to the surface. The zero energy in the potential scale denotes the vacuum level and the position scale origin denotes the z position of outermost Ir atoms. Panel (b) shows the variation of calculated binding energies for n=1 and n=2 IPS in Gr/Ir and Gr/O/Ir vs. the variation of Gr-Ir distance. The black and red vertical lines denote two specific cases of Gr-Ir distance at 3.48 and 3.80 Å, respectively. For each of the vertical line, there are four points of intersection with binding energy variation curves. These intersections indicate the binding energies for n=1 and n=2 IPS in Gr/Ir and Gr/O/Ir at the given distance, which are summarized in Table 1. Note that the relevant potentials and electron probability densities shown in (a) for Gr/Ir and Gr/O/Ir are calculated at these two distances.

We find that the increase of the Gr-Ir distance and the presence of the oxygen atoms contribute comparably in increasing the binding energies of the IPS. To illustrate this point, as shown in Table 1, if the Gr-Ir distance is increased from 3.48 Å to 3.80 Å in the absence of oxygen adatoms, the binding energy of the n=1 IPS increases by 0.09 eV from 0.77 to 0.86 eV. On the other hand, if the oxygen adatoms are present while keeping Gr-Ir distance fixed at 3.48 Å, the n=1 IPS binding energy increases by 0.10 eV from 0.77 to 0.87 eV.

In our calculations, the Gr-Ir interlayer distance is a key parameter. For Gr/Ir, the interlayer distance has been estimated by others to be in the range of 3.4-3.5 Å[28,43,44]. However, for Gr/O/Ir, no comparable experimental measurements of this interlayer distance have been reported. Here, we have used DFT calculations to estimate the change in the Gr-Ir interlayer distance before and after oxygen intercalation. The calculated interlayer distance for Gr/Ir interface was then found to be 3.48 Å which fully agrees with the experimental observation. The corresponding DFT calculation result for the Gr-Ir distance in the presence of the intercalated oxygen atoms was determined to be 3.80 Å. To probe the sensitivity of our results for the IPS binding energy predictions to the Gr-Ir interlayer distance, Fig. 4(b) shows the calculated binding energies as a function of that distance over a broad range. The influence on the n=1 state is substantial for both Gr/Ir and Gr/O/Ir cases. However, the lines run approximately parallel. This shows us that it is the change in the Gr-Ir distance upon oxygen intercalation that is the key variable. The vertical lines show the nominal cases for Gr/Ir and Gr/O/Ir based on our DFT results, with Δ=0.32 Å. If we hold Δ constant, but vary the Gr-Ir distance in the physically plausible range of 3 to 4 Å, the change in the binding energy upon oxygen intercalation is still equal to 0.20 eV within 5% variation. Note that for our calculation, the oxygen adatoms are positioned in a 2×2 lattice on the Ir surface[44]. This 2×2 oxygen distribution would give a 25% oxygen coverage in a Gr/Ir interlayer[60]. This value is consistent with those of previous reports[40,61,62].

Finally, we review the experimental observation in Fig. 2(b), where the n=2 IPS signal does not appear in the intercalated Gr/O/Ir interface. Recall that the binding energy of an IPS is pinned to the local vacuum level[63]; thus with approximately 5.12 eV measured local work function and 0.24 eV binding energy for the n=2 IPS in the Gr/O/Ir interface, its energy is expected to be approximately 4.88 eV above Fermi level. However the incident photon energy is 4.64 eV in our experiment, it was not possible to access the n=2 level, resulting in the disappearance of the n=2 IPS signal in Fig. 2(b).

V. SUMMARY

In summary, using angle-resolved two-photon-photoemission, we have probed the band structure of image potential states in quasi-free-standing graphene that is formed by oxygen-intercalation in a graphene-iridium interface. While image states have not been observed in quasi-free-standing graphene by photoemission previously, our measurements have demonstrated that IPS can be excited and probed using photoemission in a well-defined quasi-free-standing graphene system. In our experiments, the effectiveness of oxygen intercalation and the generation of quasi-free-standing Gr were determined by the loss of the LEED moiré pattern due to the decoupling of the interlayer interaction, and by the quenching of the resonant optical transitions between the oxygen-sensitive Ir surface states and the IPS. The demonstrated local sensitivity of our work function measurement allows us to measure this quantity in Gr/O/Ir domains. Our measurements show that the experimental binding energy of n=1 IPS increases from 0.79 eV in Gr/Ir to 0.96 eV in Gr/O/Ir. To understand the origin of this increased binding energy, we have developed an effective potential model, based on DFT and an empirical 1D potential model, for calculating the IPS binding energies at the Gr/Ir and Gr/O/Ir interfaces. Our model is not sensitive to any in-plane variation in the binding energy due to the negligible change of measured IPS effective mass in the oxygen intercalated sample. Within this approximation, our model is in good agreement with experimental observations. It reveals that the increased IPS binding energy in Gr/O/Ir can be attributed to an altered surface potential well due to the presence of oxygen adatoms and an increased graphene-Ir interfacial distance. The methods described here provides access to the study of surface electron dynamics in quasi-free-standing graphene. Finally, from a more general perspective, our experimental work is a further demonstration of how seemingly simple metal-adsorbate systems can exhibit a rich array of surface chemistry and physics phenomena. The number of these phenomena grow annually; see for example, a recent study of the "surface trans-effect"[64].

ACKNOWLEDGMENTS

RMO and YL acknowledge support from the US Department of Energy, Office of Basic Energy Sciences, under Contract Numbers DE-FG02-90ER14104. Our research used resources of the Center for Functional Nanomaterials, which is a U.S. DOE Office of Science Facility, at Brookhaven National Laboratory under Contract No. DE-SC0012704. We thank Dr. Denis V. Potapenko for his assistance on preparation of the sample holder and Dr. Jens Güdde for very helpful discussions of their earlier work on the graphene-Ir interface. We also thank Zhongwei Dai for very helpful discussions.

* Now at Boston University, Boston, MA 02215, USA
† Now at University of Michigan, Ann Arbor, MI 48109, USA

[1] R. Larciprete, S. Ulstrup, P. Lacovig, M. Dalmiglio, M. Bianchi, F. Mazzola, L. Hornekær, F. Orlando, A. Baraldi, P. Hofmann, *et al.*, ACS Nano **6**, 9551 (2012).
[2] I. Pletikosić, M. Kralj, P. Pervan, R. Brako, J. Coraux, A. Ndiaye, C. Busse, and T. Michely, Phys. Rev. Lett. **102**, 056808 (2009).
[3] J. Warmuth, A. Bruix, M. Michiardi, T. Hänke, M. Bianchi, J. Wiebe, R. Wiesendanger, B. Hammer, P. Hofmann, and A. A. Khajetoorians, Phys. Rev. B **93**, 165437 (2016).
[4] F. Jean, T. Zhou, N. Blanc, R. Felici, J. Coraux, and G. Renaud, Phys. Rev. B **91**, 245424 (2015).
[5] E. Voloshina, N. Berdunov, and Y. Dedkov, Sci. Rep. **6**, 20285 (2016).
[6] E. N. Voloshina, E. Fertitta, A. Garhofer, F. Mittendorfer, M. Fonin, A. Thissen, and Y. S. Dedkov, Sci. Rep. **3**, 1072 (2013).
[7] P. Sutter, P. Albrecht, X. Tong, and E. Sutter, J. Phys. Chem. C **117**, 6320 (2013).
[8] I. Pletikosić, M. Kralj, D. Šokčević, R. Brako, P. Lazić, and P. Pervan, J. Phys. Condens. Matter **22**, 135006 (2010).
[9] M. Kralj, I. Pletikosić, M. Petrović, P. Pervan, M. Milun, C. Busse, T. Michely, J. Fujii, I. Vobornik, *et al.*, Phys. Rev. B **84**, 075427 (2011).
[10] A. Varykhalov, D. Marchenko, M. Scholz, E. Rienks, T. Kim, G. Bihlmayer, J. Sánchez-Barriga, and O. Rader, Phys. Rev. Lett. **108**, 066804 (2012).
[11] P. Pervan, P. Lazić, M. Petrović, I. Š. Rakić, I. Pletikosić, M. Kralj, M. Milun, and T. Valla, Phys. Rev. B **92**, 245415 (2015).
[12] V. Dose, W. Altmann, A. Goldmann, U. Kolac, and J. Rogozik, Phys. Rev. Lett. **52**, 1919 (1984).
[13] P. Johnson and N. Smith, Phys. Rev. B **27**, 2527 (1983).
[14] K. Giesen, F. Hage, F. Himpsel, H. Riess, and W. Steinmann, Phys. Rev. Lett. **55**, 300 (1985).
[15] U. Höfer, I. Shumay, C. Reuß, U. Thomann, W. Wallauer, and T. Fauster, Science **277**, 1480 (1997).
[16] Z. Hao, J. Dadap, K. R. Knox, M. Yilmaz, N. Zaki, P. Johnson, and R. Osgood, Phys. Rev. Lett. **105**, 017602 (2010).
[17] S. Bose, V. M. Silkin, R. Ohmann, I. Brihuega, L. Vitali, C. H. Michaelis, P. Mallet, J. Y. Veuillen, M. A. Schneider, E. V. Chulkov, *et al.*, New J. Phys. **12**, 023028 (2010).
[18] M. Wolf, E. Knoesel, and T. Hertel, Phys. Rev. B **54**, R5295 (1996).
[19] P. Echenique and J. Pendry, J. Phys. C Solid State Phys. **11**, 2065 (1978).

[20] T. Fauster and W. Steinmann, Phot. Prob. Surf. **2**, 347 (1995).
[21] T. Fauster, M. Weinelt, and U. Höfer, Prog. Surf. Sci. **82**, 224 (2007).
[22] P. Echenique, R. Berndt, E. Chulkov, T. Fauster, A. Goldmann, and U. Höfer, Surf. Sci. Rep. **52**, 219 (2004).
[23] D. Niesner, T. Fauster, J. I. Dadap, N. Zaki, K. Knox, P.-C. Yeh, R. Bhandari, R. Osgood, M. Petrović, and M. Kralj, Phys. Rev. B **85**, 081402 (2012).
[24] D. Gugel, D. Niesner, C. Eickhoff, S. Wagner, M. Weinelt, and T. Fauster, 2D Materials **2**, 045001 (2015).
[25] D. Nobis, M. Potenz, D. Niesner, and T. Fauster, Phys. Rev. B **88**, 195435 (2013).
[26] D. Niesner and T. Fauster, J. Phys. Condens. Matter **26**, 393001 (2014).
[27] E. Chulkov, V. Silkin, and P. Echenique, Surf. Sci. **437**, 330 (1999).
[28] N. Armbrust, J. Güdde, and U. Höfer, New J. Phys. **17**, 103043 (2015).
[29] K. Takahashi, M. Imamura, I. Yamamoto, J. Azuma, and M. Kamada, Phys. Rev. B **89**, 155303 (2014).
[30] C. Riedl, C. Coletti, T. Iwasaki, A. Zakharov, and U. Starke, Phys. Rev. Lett. **103**, 246804 (2009).
[31] F. Speck, J. Jobst, F. Fromm, M. Ostler, D. Waldmann, M. Hundhausen, H. B. Weber, and T. Seyller, Appl. Phys. Lett. **99**, 122106 (2011).
[32] P. Sutter, J. T. Sadowski, and E. A. Sutter, J. Am. Chem. Soc. **132**, 8175 (2010).
[33] W. Jolie, F. Craes, M. Petrović, N. Atodiresei, V. Caciuc, S. Blügel, M. Kralj, T. Michely, and C. Busse, Phys. Rev. B **89**, 155435 (2014).
[34] V. Silkin, J. Zhao, F. Guinea, E. Chulkov, P. Echenique, and H. Petek, Phys. Rev. B **80**, 121408 (2009).
[35] N. Armbrust, F. Schiller, J. Güdde, and U. Höfer, Sci. Rep. **7** (2017).
[36] P. L. de Andres, P. Echenique, D. Niesner, T. Fauster, and A. Rivacoba, New J. Phys. **16**, 023012 (2014).
[37] S. J. Clark, M. D. Segall, C. J. Pickard, P. J. Hasnip, M. I. Probert, K. Refson, and M. C. Payne, Z. Kristallogr. Cryst. Mater **220**, 567 (2005).
[38] D. Vanderbilt, Phys. Rev. B **41**, 7892 (1990).
[39] Y. Xu and M. Mavrikakis, J. Chem. Phys. **116**, 10846 (2002).
[40] H. Zhang, A. Soon, B. Delley, and C. Stampfl, Phys. Rev. B **78**, 045436 (2008).
[41] B. Nieuwenhuys, R. Bouwman, and W. Sachtler, Thin Solid Films **21**, 51 (1974).
[42] F. Ortmann, F. Bechstedt, and W. Schmidt, Phys. Rev. B **73**, 205101 (2006).
[43] C. Busse, P. Lazić, R. Djemour, J. Coraux, T. Gerber, N. Atodiresei, V. Caciuc, R. Brako, S. Blügel, J. Zegenhagen, *et al.*, Phys. Rev. Lett. **107**, 036101 (2011).
[44] S. Ulstrup, M. Andersen, M. Bianchi, L. Barreto, B. Hammer, L. Hornekær, and P. Hofmann, 2D Materials **1**, 025002 (2014).
[45] M. Andersen, L. Hornekær, and B. Hammer, Phys. Rev. B **90**, 155428 (2014).
[46] R. Brako, D. Šokčević, P. Lazić, and N. Atodiresei, New J. Phys. **12**, 113016 (2010).
[47] M. Petrović, I. Š. Rakić, S. Runte, C. Busse, J. Sadowski, P. Lazić, I. Pletikosić, Z.-H. Pan, M. Milun, P. Pervan, *et al.*, Nat. Commun. **4** (2013).
[48] V. Ivanov, G. Boreskov, V. Savchenko, W. Egelhoff, and W. Weinberg, Surf. Sci. **61**, 207 (1976).
[49] S. Tognolini, S. Achilli, L. Longetti, E. Fava, C. Mariani, M. Trioni, and S. Pagliara, Phys. Rev. Lett. **115**, 046801 (2015).
[50] U. A. Schröder, M. Petrović, T. Gerber, A. J. Martínez-Galera, E. Grånäs, M. A. Arman, C. Herbig, J. Schnadt, M. Kralj, J. Knudsen, *et al.*, 2D Materials **4**, 015013 (2016).
[51] K. Giesen, F. Hage, F. Himpsel, H. Riess, W. Steinmann, and N. Smith, Phys. Rev. B **35**, 975 (1987).
[52] F. Craes, S. Runte, J. Klinkhammer, M. Kralj, T. Michely, and C. Busse, Phys. Rev. Lett. **111**, 056804 (2013).
[53] E. Starodub, N. C. Bartelt, and K. F. McCarty, J. Phys. Chem. C **114**, 5134 (2010).
[54] U. A. Schröder, E. Grånäs, T. Gerber, M. A. Arman, A. J. Martínez-Galera, K. Schulte, J. N. Andersen, J. Knudsen, and T. Michely, Carbon **96**, 320 (2016).
[55] P. Zhdan, G. Boreskov, A. Boronin, W. Egelhoff Jr, and W. Weinberg, Surface Science **61**, 25 (1976).
[56] T. S. Marinova and K. Kostov, Surface Science **185**, 203 (1987).
[57] D. Hagen, B. Nieuwenhuys, G. Rovida, and G. Somorjai, Surface Science **57**, 632 (1976).
[58] M. Bianchi, D. Cassese, A. Cavallin, R. Comin, F. Orlando, L. Postregna, E. Golfetto, S. Lizzit, and A. Baraldi, New J. Phys. **11**, 063002 (2009).
[59] E. Granas, J. Knudsen, U. A. Schroder, T. Gerber, C. Busse, M. A. Arman, K. Schulte, J. N. Andersen, and T. Michely, ACS nano **6**, 9951 (2012).
[60] C.-M. Chan and W. H. Weinberg, J. Chem. Phys. **71**, 2788 (1979).
[61] A. J. Martínez-Galera, U. Schröder, F. Huttmann, W. Jolie, F. Craes, C. Busse, V. Caciuc, N. Atodiresei, S. Blügel, and T. Michely, Nanoscale **8**, 1932 (2016).
[62] W.-H. Chung, D.-S. Tsai, L.-J. Fan, Y.-W. Yang, and Y.-S. Huang, Surf. Sci. **606**, 1965 (2012).
[63] S. Smadici and R. M. Osgood, Phys. Rev. B **71**, 165424 (2005).
[64] P. S. Deimel, R. M. Bababrik, B. Wang, P. J. Blowey, L. A. Rochford, P. K. Thakur, T.-L. Lee, M.-L. Bocquet, J. V. Barth, D. P. Woodruff, *et al.*, Chemical Science **7**, 5647 (2016).